

# Black hole growth in the early Universe is self-regulated and largely hidden from view

Ezequiel Treister<sup>1,2,3</sup>, Kevin Schawinski<sup>2,4,5</sup>, Marta Volonteri<sup>6</sup>, Priyamvada Natarajan<sup>4,5,7,8</sup> and Eric Gawiser<sup>9</sup>

October 31, 2018

<sup>1</sup>Institute for Astronomy, 2680 Woodlawn Drive, University of Hawaii, Honolulu, HI 96822 <sup>2</sup>Chandra/Einstein Fellow <sup>3</sup>Universidad de Concepción, Departamento de Astronomía, Casilla 160-C, Concepción, Chile <sup>4</sup>Yale Center for Astronomy and Astrophysics, P.O. Box 208121, New Haven, CT 06520. <sup>5</sup>Department of Physics, Yale University, P.O. Box 208121, New Haven, CT 06520. <sup>6</sup>Department of Astronomy, University of Michigan, Ann Arbor, Michigan 48109, USA. <sup>7</sup>Department of Astronomy, Yale University, PO Box 208101, New Haven, CT 06520. <sup>8</sup>Institute for Theory and Computation, Harvard University, 60 Garden Street, Cambridge, MA 02138. <sup>9</sup>Department of Physics and Astronomy, Rutgers University, 136 Frelinghuysen Road, Piscataway, NJ 08854

The formation of the first massive objects in the infant Universe remains impossible to observe directly and yet it sets the stage for the subsequent evolution of galaxies<sup>1,2,59</sup>. While some black holes with masses  $>10^9 M_\odot$  have been detected in luminous quasars less than one billion years after the Big Bang<sup>5,65</sup>, these individual extreme objects have limited utility in constraining the channels of formation of the earliest black holes. The initial conditions of black hole seed properties are quickly erased during the growth process<sup>6</sup>. From deep, optimally-stacked, archival X-ray observations, we measure the amount of black hole growth in  $z=6-8$  galaxies (0.7-1 billion years after the Big Bang). Our results imply that black holes grow in tandem with their hosts throughout cosmic history, starting from the earliest times. We find that most copiously accreting black holes at these epochs are buried in significant amounts of gas and dust that absorb most radiation except for the highest energy X-rays. This suggests that black holes grow significantly more than previously thought during these early bursts, and due to obscuration they do not contribute to the re-ionization of the Universe with their ultraviolet emission.

The *Chandra* X-ray observatory is sensitive to photons in the energy range 0.5-8 keV, which in deep extragalactic observations probes predominantly accretion onto supermassive black holes<sup>7</sup>. Rapidly growing black holes are known to be surrounded by an obscuring medium, which can block most of the optical, ultra-violet and even soft X-ray photons<sup>8</sup>. With increasing redshift, at the earliest epochs, the photons observed by *Chandra* are emitted at intrinsically higher energies, and therefore less affected by such absorption. Current X-ray observations have not been able to individually detect most of the first black hole growth events at  $z>6$  (first 950 million years after the Big Bang) thus far, except for the most luminous quasars<sup>9</sup> at  $L_X > 3 \times 10^{44}$  erg s<sup>-1</sup>. While deep X-ray surveys do not cover enough volume at high redshift, current wide-area studies are simply not deep enough. Hence, the only way to obtain a detectable signal from more typical growing black holes is by adding the X-ray emission from a large number of sources at these redshifts, which we pursue here.

We start by studying the collective X-ray emission from the most distant galaxies known, at  $z\sim 6$ <sup>31</sup>,  $z\sim 7$ <sup>32</sup> and  $z\sim 8$ <sup>12</sup>, detected by the Wide Field Camera aboard the *Hubble* Space Telescope. These galaxies are as massive as today's galaxies ( $10^9 - 10^{11} M_\odot$  stellar mass<sup>13</sup>), and they

are thus likely to harbor substantial nuclear black holes. None of the  $z>6$  galaxies studied in this work are individually detected in the *Chandra* X-ray observations. However, we detect significant signals from a stack of 197 galaxies at  $z\sim 6$  in both the soft (0.5-2.0 keV; corresponding to 3.5-14 keV in the rest frame) and hard (2-8 keV; rest-frame 14-56 keV) X-ray bands independently. The detection in the soft band is significant at the 5- $\sigma$  level and implies an average observed-frame luminosity of  $9.2 \times 10^{41}$  erg s<sup>-1</sup>, while in the hard band the stacked 6.8- $\sigma$  signal corresponds to an average luminosity of  $8.4 \times 10^{42}$  erg s<sup>-1</sup>. For the sample of galaxies at  $z\sim 7$  we obtain 3- $\sigma$  upper limits for the average luminosity in the observed-frame soft and hard X-ray bands of  $4 \times 10^{42}$  erg s<sup>-1</sup> and  $2.9 \times 10^{43}$  erg s<sup>-1</sup> respectively. Combining the  $z\sim 7$  and  $z\sim 8$  samples the corresponding 3- $\sigma$  upper limits are  $3.1 \times 10^{42}$  erg s<sup>-1</sup> and  $2.2 \times 10^{43}$  erg s<sup>-1</sup> in the observed-frame soft and hard X-ray bands.

A large difference, of a factor of  $\sim 9$ , is found between the stacked fluxes in the soft and hard X-ray bands at  $z \sim 6$ . This requires large amounts of obscuring material with high columns ( $N_H > 1.6 \times 10^{24}$  cm<sup>-2</sup>) to be present in a very high fraction of the accreting black holes in these galaxies, in order to explain the large deficit of soft X-ray photons. Since this signal derives from the entire population, these results require that almost all sources are significantly obscured. This in turn implies that these growing black holes are obscured along most lines of sight, as observed in a small subset of nearby objects<sup>39</sup> as well. Such high fraction of obscured sources at low luminosities is also observed at low redshifts<sup>42</sup>. This large amount of obscuration along all directions absorbs virtually all ultraviolet photons from growing black holes. Thus, regardless of the amount of accretion in these sources, these active galaxies cannot contribute to the early re-ionization of the Universe. Alternatively, it cannot be claimed that rapid and efficient supermassive black hole growth in the high- $z$  Universe is implausible on the basis of any re-ionization constraints<sup>16</sup>. If most of the high-redshift black hole growth is indeed obscured as suggested by our work, several current constraints on the lifetime and duty cycle of high- $z$  accreting black holes need to be revisited and revised.

Assuming that the X-ray emission is due to accretion onto the central black hole, the accreted black hole mass density can be directly derived from the observed X-ray luminosity, as described in the supplementary information. Extrapolations of Active Galactic Nuclei (AGN) luminosity functions<sup>58</sup> measured at significantly lower redshifts,  $z<3$ , are consistent with the observed accreted black hole mass density at  $z>6$ , as can be seen in Figure 1. This directly leads to two further conclusions: the space density of low luminosity sources,  $L_X < 10^{44}$  erg s<sup>-1</sup>, does not evolve significantly from  $z\sim 1$  to  $z\sim 6-8$ , i.e. over more than 5 billion years. Second, at higher luminosities, the extrapolation of lower-redshift AGN luminosity functions leads to an overestimate of the observed source density in optical surveys<sup>57</sup>. This discrepancy can be resolved if the shape of the AGN luminosity function evolves strongly in the sense that there are relatively fewer high-luminosity AGN at  $z>6$  in comparison to the  $z<3$  population.

Another possibility is that the number of obscured sources, relative to unobscured quasars, increases with redshift, such that most of the highly obscured systems are systematically missed in these optical studies. This is strongly supported by observations of quasars at lower redshifts,  $z < 3^{66}$ . We cannot rule out either of these scenarios at present due to the relatively small cosmological volume studied, in which the extremely rare high-luminosity AGN are absent.

Our measurements and upper limits for the accreted black hole mass density up to  $z \sim 8.5$  ( $\sim 600$  million years after the Big Bang) constrain the nature of black hole growth in the early Universe. Two critical issues for AGN and the supermassive black holes powering them are how the first black holes formed, and how they subsequently grew accreting mass while shining as AGN. The strong local correlation between black hole mass and galaxy bulge mass observed at  $z \sim 0^{20,21}$ , is interpreted as evidence for self-regulated black hole growth and galaxy-black hole co-evolution<sup>1,22</sup>. This is currently the default assumption for most galaxy formation and evolution models<sup>23,24</sup>.

The origin of the initial “seed” black holes remains an unsolved problem at present. Two channels to form these seeds have been proposed: compact remnants of the first stars, the so-called population III stars<sup>25</sup>, which generate seeds with masses  $\sim 10\text{--}1,000 M_{\odot}$  and from the direct gravitational collapse of gas-rich pre-galactic disks, which leads to significantly more massive seeds with masses in the range  $M \sim 10^5 M_{\odot}$ <sup>26,27</sup>. By construction, the masses of seeds that form from direct collapse are correlated to properties of the dark matter halo and hence properties of the galaxy that will assemble subsequently.

To interpret our finding, we explore a theoretical framework for the cosmic evolution of supermassive black holes in a  $\Lambda$ CDM cosmology. We follow the formation and evolution of black holes through dedicated Monte Carlo merger tree simulations. Each model is constructed by tracing the merger hierarchy of dark matter halos in the mass range  $10^{11} - 10^{15} M_{\odot}$  backwards to  $z = 20$ , using an extended Press & Schechter algorithm<sup>59</sup>. The halos are then seeded with black holes and their evolution is tracked forward to the present time. Following a major merger (defined as a merger between two halos with mass ratio  $> 0.1$ ), supermassive black holes accrete efficiently an amount of mass that is set by a “self-regulated” model (where the accreted mass scales with the fourth power of the host halo circular velocity and is normalized to reproduce the observed local correlation between supermassive black hole mass and velocity dispersion) or a “un-regulated” model, where the supermassive black hole simply doubles in mass at each accretion episode. See the Supplementary Information for additional details.

Our observational results provide strong support for the existence of a correlation between supermassive black holes and their hosts out to the highest redshifts. In Figure 1, we compare both unregulated and self-regulated black hole growth models with our observations, and find that physically motivated self-regulation growth models are highly favored at all redshifts, even in the very early Universe. Un-regulated models (for instance wherein black holes just double in mass at each major merger) are strongly disfavored by the data. This indicates that even in the first episodes of black hole growth there is a fundamental link between galaxy and black hole mass assembly.

As shown in Figure 1, once a standard prescription for self-regulation (as described before) is incorporated, both seed models are consistent with our current high- $z$  observations. Detection of an unbiased population of sources at these early epochs is the one metric that we have in the foreseeable future to distinguish between these two scenarios for the origin of supermassive black holes in the Universe. In Figure 2, we present the predicted cumulative source counts at  $z > 6$  for the models studied here. Based on these models, ultra-deep X-ray and near-infrared surveys covering at least  $\sim 1 \text{ deg}^2$  are required to constrain the formation of the first black hole seeds. This will likely require the use of the next generation of space-based observatories such as the James Webb Space Telescope and

the International X-ray Observatory.

## References

1. Silk, J. & Rees, M. J. Quasars and galaxy formation. *Astron. Astrophys.* **331**, L1–L4 (1998).
2. Barkana, R. & Loeb, A. In the beginning: the first sources of light and the reionization of the universe. *Phys. Rep.* **349**, 125–238 (2001).
3. Volonteri, M., Haardt, F. & Madau, P. The Assembly and Merging History of Supermassive Black Holes in Hierarchical Models of Galaxy Formation. *Astrophys. J.* **582**, 559–573 (2003).
4. Fan, X. *et al.* High-Redshift Quasars Found in Sloan Digital Sky Survey Commissioning Data. IV. Luminosity Function from the Fall Equatorial Stripe Sample. *Astron. J.* **121**, 54–65 (2001).
5. Willott, C. J. *et al.* Four Quasars above Redshift 6 Discovered by the Canada-France High- $z$  Quasar Survey. *Astron. J.* **134**, 2435–2450 (2007).
6. Volonteri, M. & Rees, M. J. Quasars at  $z=6$ : The Survival of the Fittest. *Astrophys. J.* **650**, 669–678 (2006).
7. Brandt, W. N. & Hasinger, G. Deep Extragalactic X-Ray Surveys. *Ann. Rev. Astron. Astrophys.* **43**, 827–859 (2005).
8. Lawrence, A. & Elvis, M. Obscuration and the various kinds of Seyfert galaxies. *Astrophys. J.* **256**, 410–426 (1982).
9. Shemmer, O. *et al.* Chandra Observations of the Highest Redshift Quasars from the Sloan Digital Sky Survey. *Astrophys. J.* **644**, 86–99 (2006).
10. Bouwens, R. J., Illingworth, G. D., Blakeslee, J. P. & Franx, M. Galaxies at  $z \sim 6$ : The UV Luminosity Function and Luminosity Density from 506 HUDF, HUDF Parallel ACS Field, and GOODS i-Dropouts. *Astrophys. J.* **653**, 53–85 (2006).
11. Bouwens, R. J. *et al.* UV Luminosity Functions from 113  $z \sim 7$  and  $z \sim 8$  Lyman-Break Galaxies in the ultra-deep HUDF09 and wide-area ERS WFC3/IR Observations. *ArXiv e-prints*, 1006.4360 (2010).
12. Bouwens, R. J. *et al.* Discovery of  $z \sim 8$  Galaxies in the Hubble Ultra Deep Field from Ultra-Deep WFC3/IR Observations. *Astrophys. J.* **709**, L133–L137 (2010).
13. Labbé, I., Bouwens, R., Illingworth, G. D. & Franx, M. Spitzer IRAC Confirmation of  $z_{850}$ -Dropout Galaxies in the Hubble Ultra Deep Field: Stellar Masses and Ages at  $z \sim 7$ . *Astrophys. J.* **649**, L67–L70 (2006).
14. Ueda, Y. *et al.* Suzaku Observations of Active Galactic Nuclei Detected in the Swift BAT Survey: Discovery of a “New Type” of Buried Supermassive Black Holes. *Astrophys. J.* **664**, L79–L82 (2007).
15. Sazonov, S., Revnivtsev, M., Krivonos, R., Churazov, E. & Sunyaev, R. Hard X-ray luminosity function and absorption distribution of nearby AGN: INTEGRAL all-sky survey. *Astron. Astrophys.* **462**, 57–66 (2007).
16. Loeb, A. The race between stars and quasars in reionizing cosmic hydrogen. *J. Cosmology Astropart. Phys.* **3**, 22–+ (2009).
17. Treister, E., Urry, C. M. & Virani, S. The Space Density of Compton Thick AGN and the X-ray Background. *Astrophys. J.* **696**, 110–120 (2009).
18. Willott, C. J. *et al.* The Canada-France High- $z$  Quasar Survey: Nine New Quasars and the Luminosity Function at Redshift 6. *Astron. J.* **139**, 906–918 (2010).
19. Treister, E. *et al.* Major Galaxy Mergers and the Growth of Supermassive Black Holes in Quasars. *Science* **328**, 600– (2010).
20. Ferrarese, L. & Merritt, D. A Fundamental Relation between Supermassive Black Holes and Their Host Galaxies. *Astrophys. J.* **539**, L9–L12 (2000).
21. Gebhardt, K. *et al.* A Relationship between Nuclear Black Hole Mass and Galaxy Velocity Dispersion. *Astrophys. J.* **539**, L13–L16 (2000).
22. King, A. Black Holes, Galaxy Formation, and the  $M_{BH}-\sigma$  Relation. *Astrophys. J.* **596**, L27–L29 (2003).
23. Wyithe, J. S. B. & Loeb, A. Self-regulated Growth of Supermassive Black Holes in Galaxies as the Origin of the Optical and X-Ray Luminosity Functions of Quasars. *Astrophys. J.* **595**, 614–623 (2003).
24. Hopkins, P. F. *et al.* A Unified, Merger-driven Model of the Origin of Starbursts, Quasars, the Cosmic X-Ray Background, Supermassive Black Holes, and Galaxy Spheroids. *Astrophys. J.* **163**, 1–49 (2006).
25. Madau, P. & Rees, M. J. Massive Black Holes as Population III Remnants. *Astrophys. J.* **551**, L27–L30 (2001).
26. Bromm, V. & Loeb, A. Formation of the First Supermassive Black Holes. *Astrophys. J.* **596**, 34–46 (2003).
27. Lodato, G. & Natarajan, P. Supermassive black hole formation during the assembly of pre-galactic discs. *Mon. Not. R. Astron. Soc.* **371**, 1813–1823 (2006).
28. Shankar, F., Weinberg, D. H. & Miralda-Escudé, J. Self-Consistent Models of the AGN and Black Hole Populations: Duty Cycles, Accretion Rates, and the Mean Radiative Efficiency. *Astrophys. J.* **690**, 20–41 (2009).
29. Treister, E., Urry, C. M., Schawinski, K., Cardamone, C. N. & Sanders, D. B. Heavily Obscured Active Galactic Nuclei in High-redshift Luminous Infrared Galaxies. *Astrophys. J.* **722**, L238–L243 (2010).
30. Volonteri, M. Formation of supermassive black holes. *Astron. Astrophys. Rev.* **18**, 279–315 (2010).

**Supplementary Information** is linked to the online version of the paper at <http://www.nature.com/nature>.

**Acknowledgments** We thank Tomo Goto, Meg Urry and Dave Sanders for very insightful conversations. Support for the work of ET and KS was provided NASA through *Chandra*/Einstein Post-doctoral Fellowship Awards. MV acknowledges support from the Smithsonian Astrophysical Observatory. PN acknowledges support via a Guggenheim Fellowship from the John Simon Guggenheim Foundation. The work of EG was partially funded by NSF.

**Author Contributions** E.T. started the project, collected the galaxy samples, performed the X-ray stacking calculations and wrote the majority of the text. K.S. helped to collect the galaxy sample studied here, contributed to the conception of the project, the analysis and interpretation of the results. M.V. and P.N. created the black hole growth models, computed the contribution of these sources to the re-ionization of the Universe and contributed extensively to the theoretical interpretation of the observational results. E.G. developed the optimal X-ray stacking formalism and worked with E.T. to implement it on these data. All authors discussed the results and contributed to the writing of the manuscript.

**Competing Interests** The authors declare that they have no competing financial interests.

**Correspondence** Correspondence and requests for materials should be addressed to E. Treister. (email: [treister@ifa.hawaii.edu](mailto:treister@ifa.hawaii.edu)).

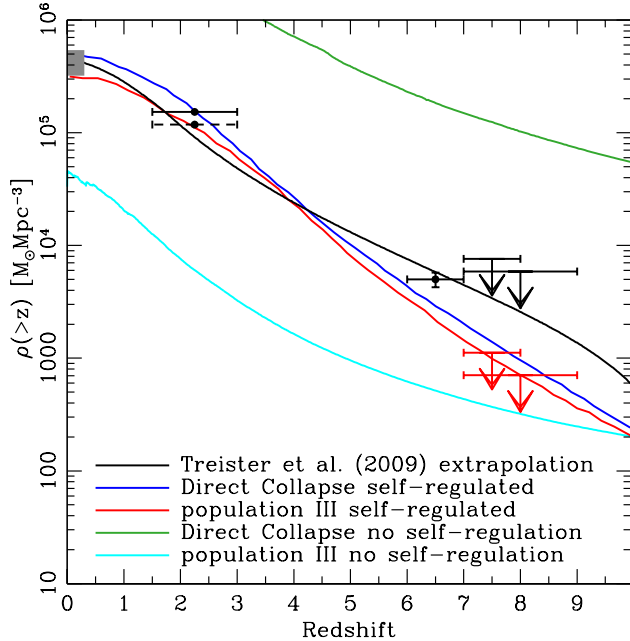


**Figure 1** | Accreted black hole mass density as a function of redshift. The gray rectangle shows the range of values allowed by observations of  $z \sim 0$  galaxies<sup>53</sup>. The data points at  $z \sim 2$  correspond to the values obtained from *Chandra* observations of X-ray detected AGN and luminous infrared galaxies<sup>54</sup>, while the measurement at  $z \sim 6$  and the upper limits at  $z = 7-9$  show the results described in this work (red and black data points from the observed-frame soft and hard X-ray band observations respectively). Vertical error bars represent 1 s.d. while the horizontal ones show the bin size. The black solid line shows the evolution of the accreted black hole mass density inferred from the extrapolation of AGN luminosity functions measured at lower redshifts<sup>58</sup>. We over-plot the predictions of black hole and galaxy evolution models<sup>30</sup> for non-regulated growth of Population-III star remnants (cyan line) and direct-collapse seeds (green). The red and blue lines show the predicted BH mass density if self-regulation is incorporated.

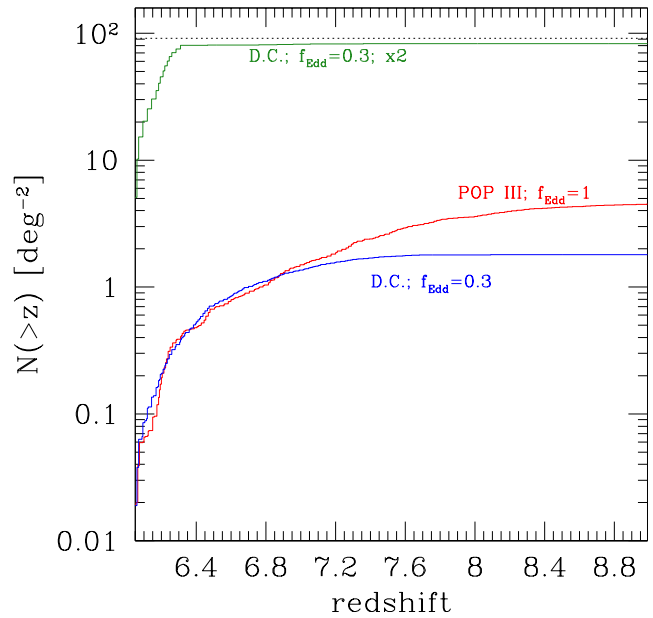


**Figure 2** | Cumulative number of sources as a function of redshift for individual X-ray detections. This calculation assumes the X-ray flux limit of the 4 Msec CDF-S *Chandra* observations. The horizontal dotted line shows the number density required to individually detect one source in the area considered in this work at  $z > 7$ . Models are described in the supplemental material and labelled in the figure (Pop III,  $f_{\text{Edd}} = 1$ ; D.C.,  $f_{\text{Edd}} = 0.3$ ; D.C.,  $f_{\text{Edd}} = 0.3, \times 2$ ). Note: model Pop III,  $f_{\text{Edd}} = 1, \times 2$  has no detectable source. To distinguish between these models for early black hole formation will require a deep multiwavelength survey covering at least  $\sim 1 \text{ deg}^2$ .

## Supplementary Information

### The Observations

The main observational data samples for this work are the 371 galaxy candidates at  $z\sim 6$  selected using the optical and near-IR Lyman break technique<sup>31</sup>, together with 66  $z\sim 7$  and 47  $z\sim 8$  galaxy candidates<sup>32</sup>, all of them in the *Chandra* Deep Field South (CDF-S) field. We then complemented this sample with the 151  $z\sim 6$  candidates in the *Chandra* Deep Field North (CDF-N)<sup>31</sup>. The accuracy of this drop-out technique selection has been recently confirmed by spectroscopic observations of some of these sources<sup>33–35</sup>. The contamination by foreground sources in these samples appears to be very small,  $\sim 10\%$ <sup>32,33</sup>. We then used the 4 Msec *Chandra* observations of the CDF-S<sup>36</sup> and the 2 Msec *Chandra* data available on the CDF-N<sup>37</sup> in order to search for signatures of supermassive black hole (SMBH) accretion in these sources. None of these galaxies are detected individually in the X-ray data. However, *Chandra* data are uniquely suited to perform stacking, which allows us to reach much fainter flux limits. In order to maximize the signal-to-noise of these measurements we used an optimized X-ray stacking scheme, described in detail in Appendix A. We stack independently in the soft, 0.5–2 keV, and hard, 2–8 keV, observed-frame *Chandra* bands. At  $z\sim 7$ , they correspond to rest-frame energies of 4–16 and 16–64 keV respectively. While at these high rest-frame energies the effects of Compton-thin obscuration ( $N_H < 10^{24} \text{ cm}^{-2}$ ) are negligible, we have to consider the possibility of higher absorption column densities. We restricted our stack to sources closer than  $\sim 9'$  from the average aim point of the *Chandra* observations in order to have an optimal extraction radius smaller than  $7''$  (Fig. S3). We further removed sources with an X-ray detection closer than  $22''$  to avoid possible contamination in the background determination.

In the sample of candidates at  $z\sim 6$  we stacked a total of 197 sources, 151 in the CDF-S and 46 in the CDF-N. This corresponds to a total exposure time of  $\sim 7 \times 10^8$  seconds ( $\sim 23$  years). We found significant detections,  $\geq 5\text{-}\sigma$ , in both the soft and hard bands independently. In the soft band we computed a count rate of  $3.4 \pm 0.68 \times 10^{-7}$  counts  $\text{s}^{-1}$  per source, which corresponds to an observed-frame soft band flux of  $2.3 \times 10^{-18}$  erg  $\text{cm}^{-2} \text{s}^{-1}$ . Converting it to the rest-frame hard band we obtain a flux of  $1.9 \times 10^{-18}$  erg  $\text{cm}^{-2} \text{s}^{-1}$ . In the observed-frame hard band we measure a count rate of  $8.8 \pm 1.3 \times 10^{-7}$  counts  $\text{s}^{-1}$ , which corresponds to a  $6.8\text{-}\sigma$  detection. The average flux in the observed-frame hard band is  $2.1 \times 10^{-17}$  erg  $\text{cm}^{-2} \text{s}^{-1}$ , which converted to the rest-frame hard-band corresponds to  $1.7 \times 10^{-17}$  erg  $\text{cm}^{-2} \text{s}^{-1}$ . Stacked *Chandra* images for this sample in the soft and hard X-ray bands are shown in Fig. S4

There is a factor  $\sim 9$  difference between the fluxes measured in the observed-frame soft and hard bands. Assuming a power-law X-ray spectrum with an intrinsic spectral slope  $\Gamma=1.9$ , typical of AGN<sup>38</sup>, the expected flux ratio between the observed-frame soft and hard bands for an unobscured source is expected to be  $\sim 1.7$  (Fig. S5). The only explanation for the relatively large flux ratio in the hard to soft bands is very high levels of obscuration. As can be seen in Fig. S5, at  $z\sim 6$  a minimum column density of  $N_H \simeq 10^{24} \text{ cm}^{-2}$ , i.e. Compton-thick obscuration, is required. Given that this ratio is observed in the stack, this implies that there are very few sources with significantly lower levels of obscuration, which in turn means that these sources must be nearly Compton-thick along most directions ( $\sim 4\pi$  obscuration). Similar sources have also been observed in the local Universe<sup>39</sup> but are likely rare. Furthermore, up to  $z\sim 3$  it has been shown before<sup>40–42</sup> that the fraction of obscured AGN increases with decreasing luminosity and increasing redshift<sup>43,44</sup>. Hence, it is not entirely surprising that the sources studied here, given their low luminosities and high redshifts, are heavily obscured. In fact, the discovery of a Compton-thick AGN at  $z\sim 5$  selected using the drop-out technique has been recently reported<sup>45</sup>.

The corresponding average rest-frame 2–10 keV luminosity, derived from the observed-frame hard band, is  $6.8 \times 10^{42}$  erg  $\text{s}^{-1}$ . Since none

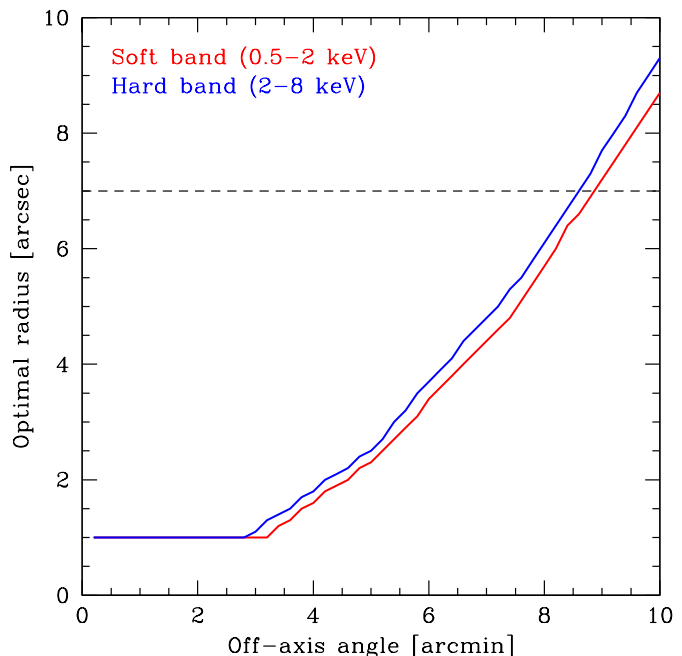


**Figure 3** | Optimal extraction radius as a function of off-axis angle, measured from the average *Chandra* pointing center. As described in the appendix A, these lines were measured by optimizing the function  $f(\theta, r)/r$ . A minimum radius of  $1''$  was assumed in order to avoid flux losses due to astrometric problems and pixel aliasing. Red and blue lines show the optimal radii for the soft and hard band respectively. Sources with optimal radii greater than  $7''$  (dashed horizontal line) are not considered in the stack, given their low expected contribution to the integrated signal-to-noise.

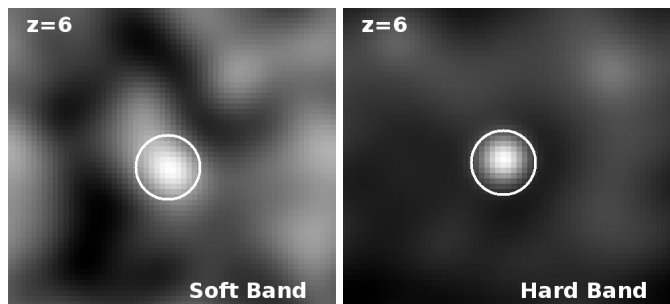


**Figure 4** | Stacked *Chandra* images for the  $z=6$  galaxy sample in the soft (left panel) and hard (right panel) X-ray bands. The detections are significant at the 5 and  $6.8\text{-}\sigma$  levels respectively. Each image is  $30'' \times 30''$ . The white circle at the center of each image has a radius of  $3''$ . Images were adaptively smoothed using a minimum scale of 3 pixels, a maximum scale of 5 pixels and minimum and maximum significances of 3 and 6 respectively.

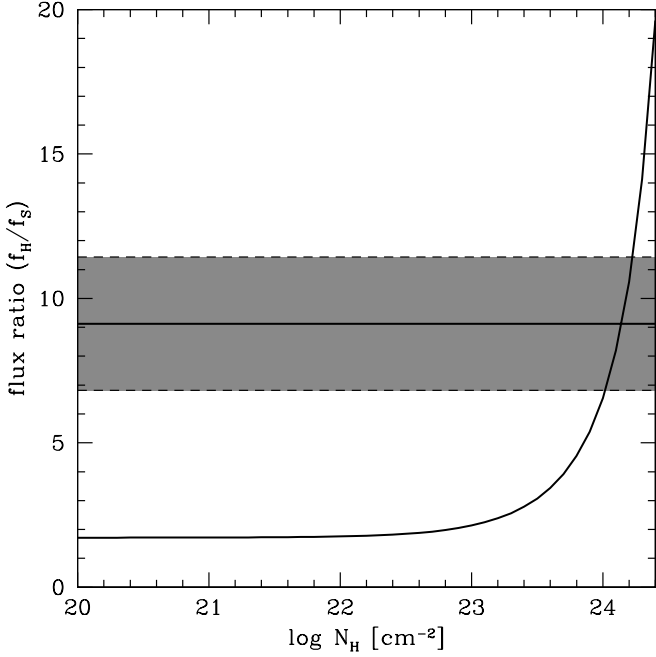


**Figure 5** | Expected ratio of the observed-frame hard to soft flux as a function of obscuring neutral Hydrogen column density ( $N_H$ ). The *black solid line* was derived assuming an intrinsic power-law spectrum with slope  $\Gamma=1.9$  and photoelectric absorption. The gray zone shows the measured ratio for the stack of galaxies at  $z\sim 6$  and the  $\pm 1$  s.d. limits. A column density of  $N_H\sim 10^{24}$   $\text{cm}^{-2}$ , i.e. Compton-thick obscuration, is required to explain the observed hard to soft X-ray flux ratio.

of these sources are individually detected in X-rays, we conclude that at least 30% of the galaxies in this sample contain an AGN. Multiplying by the number of sources we obtain a total luminosity of  $1.34\times 10^{45}$   $\text{erg s}^{-1}$ . The total area surveyed is  $\sim 310$   $\text{arcmin}^2$ , or  $0.086$   $\text{deg}^2$ . Hence, the integrated AGN emissivity at  $z\sim 6$  derived from this sample is  $1.6\times 10^{46}$   $\text{erg s}^{-1}\text{deg}^{-2}$ .

Similarly, we stacked a total of 57 sources by combining the samples at  $z>7$  and  $z>8$ . For the galaxies in this redshift range, we found no significant detection in the observed-frame soft or hard bands. The  $3\text{-}\sigma$  upper limits are  $6.9\times 10^{-7}$   $\text{cts s}^{-1}$  and  $1.4\times 10^{-6}$   $\text{cts s}^{-1}$ , which corresponds to flux upper limits of  $4.6\times 10^{-18}$   $\text{erg cm}^{-2}\text{s}^{-1}$  and  $3.3\times 10^{-17}$   $\text{erg cm}^{-2}\text{s}^{-1}$  respectively. Assuming an average redshift  $z=7.5$  and converting to the rest-frame hard band, 2-10 keV, we obtain average luminosities of  $3.1\times 10^{42}$   $\text{erg s}^{-1}$  and  $2.2\times 10^{43}$   $\text{erg s}^{-1}$  from the observed-frame soft and hard band respectively. Because we only have upper limits in both bands, we cannot constrain the presence of obscuration in this sample, however assuming that these AGN are as heavily obscured as the  $z\sim 6$  sample, the shallower limit from the hard band is actually the more stringent constraint. The area covered in the  $z>7$  observations is  $40$   $\text{arcmin}^2$ , or  $0.011$   $\text{deg}^2$ . Hence, the upper limits to the integrated AGN emissivity are  $5.2\times 10^{45}$   $\text{erg s}^{-1}\text{deg}^{-2}$  and  $4.3\times 10^{46}$   $\text{erg s}^{-1}\text{deg}^{-2}$  respectively.

Finally, we also stacked the galaxies in the  $z\sim 7$  sample separately. In this case we obtained  $3\text{-}\sigma$  upper limits of  $6.9\times 10^{-18}$   $\text{erg cm}^{-2}\text{s}^{-1}$  and  $5.0\times 10^{-17}$   $\text{erg cm}^{-2}\text{s}^{-1}$  in the observed frame soft and hard bands respectively. These correspond to average observed-frame luminosities of  $4.0\times 10^{42}$   $\text{erg s}^{-1}$  and  $2.9\times 10^{43}$   $\text{erg s}^{-1}$ . Dividing by the survey area and multiplying by the number of sources we obtain  $3\text{-}\sigma$  upper limits for the integrated AGN emissivities from these galaxies of  $4.3\times 10^{45}$   $\text{erg s}^{-1}\text{deg}^{-2}$  and  $2.9\times 10^{46}$   $\text{erg s}^{-1}\text{deg}^{-2}$  respectively.

## Black Hole Mass Density Determination

We compute the observed integrated black hole mass density using an updated version of the ‘‘Soltan’’<sup>46</sup> argument. Following the standard derivations<sup>47,48</sup> we have that the integrated black hole mass density is given by:

$$\rho_{BH}(z) = \int_z^\infty \frac{dt}{dz} dz \int_0^\infty \frac{1-\epsilon}{\epsilon c^2} L_{bol} \Psi(L, z) dL, \quad (1)$$

where

$$L_{bol} = k_{corr} L_X \quad (2)$$

and  $k_{corr}$  is the bolometric correction for the rest-frame hard X-ray band. In order to compute  $\rho_{BH}(z)$  we need to make some assumptions, since the AGN luminosity function (LF) at  $z>6$  is unknown, and only the integrated luminosity is known. First, we assume that at  $z>6$  the AGN LF does not depend strongly on redshift, i.e.,  $\Psi(L, z)\simeq\Psi(L)$ . We further assume that the efficiency and bolometric corrections are constant (i.e., independent of luminosity). While we know that the bolometric correction depends on luminosity<sup>48,49</sup>, our sample most likely does not span a wide luminosity range, and hence this assumption is reasonable. Therefore, we have,

$$\rho_{BH}(z) = \frac{(1-\epsilon)k_{corr}}{\epsilon c^2} \int_z^\infty \frac{dt}{dz} dz \int_0^\infty L_X \Psi(L) dL. \quad (3)$$

The second integral on the right hand side can be determined from the observed integrated AGN emissivity. We only need to convert from a density per unit of sky area (the observed value) to a co-moving AGN emissivity per unit of volume. This can be done easily by dividing the observed value by the co-moving volume at the redshift range covered by each sample. In principle, a correction should be made to account for the contribution of high-luminosity sources not present in the relatively narrow fields considered in this work. However, as we will show below, this correction should be small,  $\sim 1\text{-}2\%$ , and thus can be safely ignored.

The bolometric correction  $k_{corr}$  has been estimated by several authors in the past. For high-luminosity sources (quasars), a value of 35 was measured<sup>50</sup>. For low-luminosity sources,  $L_x\sim 10^{43}$   $\text{erg s}^{-1}$ , values of  $\sim 10\text{-}20$ , were estimated<sup>48</sup>, while newer calculations<sup>51</sup> report a value of  $\sim 25$  for sources with  $L_x\sim 10^{42}$   $\text{erg s}^{-1}$  and  $\sim 40$  at  $L_x\sim 10^{43}$   $\text{erg s}^{-1}$ . Given the low luminosity of the sources in our sample we assume a value of  $k_{corr}=25$ , with an estimated uncertainty of a factor of  $\sim 2$ . The main factor contributing to this uncertainty is the determination of the contribution of the X-ray emission relative to the ultraviolet (where most of the bolometric output is found). Observational studies show that this factor depends on luminosity but remains constant with redshift up to  $z\sim 6$ <sup>52</sup>.

Assuming a constant radiation efficiency  $\epsilon=0.1$  we obtain from the combined  $z=7\text{-}8$  sample  $3\text{-}\sigma$  upper limits of  $\rho_{BH}<708$   $M_\odot\text{Mpc}^{-3}$  (possibly affected by obscuration) and  $\rho_{BH}<5883$   $M_\odot\text{Mpc}^{-3}$  from the observed-frame soft and hard band respectively.

For the sample of galaxies at  $z\sim 7$  only, assuming that all these galaxies lie between  $z_1=7$  and  $z_2=8$ , we obtain that  $\rho_{BH}<1117$   $M_\odot\text{Mpc}^{-3}$  from the observed-frame soft-band and  $\rho_{BH}<7595$   $M_\odot\text{Mpc}^{-3}$  from the hard band. Finally, for our sample of  $z\sim 6$  galaxy candidates we obtain from the stacked detection in the observed-frame hard band that  $\rho_{BH}=5005\pm 751$   $M_\odot\text{Mpc}^{-3}$  ( $1\text{-}\sigma$ ).

In Figure S6 we plot the integrated accreted black hole mass density as a function of redshift. The upper limits at  $z\sim 7\text{-}8$  and measurement at  $z\sim 6$  obtained from our work are shown together with the observations in the local Universe<sup>53</sup> and the values derived from *Chandra* observations of X-ray detected AGN and luminous infrared galaxies at  $z\sim 2$ <sup>54</sup>.

## Accretion Models: key features

We investigate the formation and evolution of black holes via cosmological realizations of the merger hierarchy of dark matter halos from early

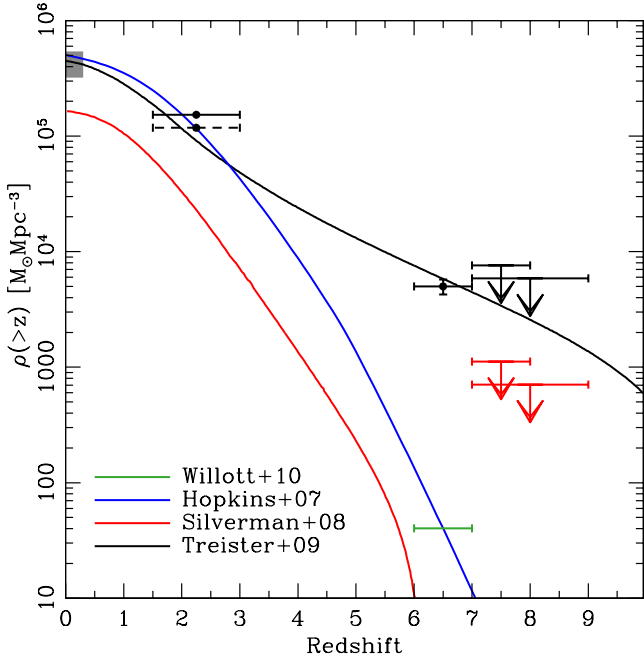


**Figure 6** | Accreted black hole mass density as a function of redshift. The gray rectangle shows the range of values allowed by observations of  $z \sim 0$  galaxies<sup>53</sup>. The data points at  $z \sim 2$  correspond to the values obtained from *Chandra* observations of X-ray detected AGN and luminous infrared galaxies<sup>54</sup>, while the measurements at  $z \sim 6$  and the upper limits at  $z = 7-9$  show the results described in this work (red and black data points from the observed-frame soft and hard X-ray band observations respectively). The red and blue lines show the values inferred from AGN luminosity functions<sup>55,56</sup>, while the point at  $z = 6-7$  was obtained from the quasar luminosity function<sup>57</sup>. The black line assumes the hard X-ray AGN LF of Ueda et al.<sup>40</sup>, as modified by Treister et al.<sup>58</sup>.

times to the present in a  $\Lambda$ CDM cosmology. The main features of the by now fairly standard SMBH evolution models that are used to interpret the data have been discussed in detail elsewhere<sup>59-61</sup>. We briefly outline some of the key features here. In this work, two “seed” formation models are considered: those deriving from population-III star remnants (Pop III), and from direct collapse models (D.C.). The main difference between these two models lies in the mass function of seeds. Pop III seeds are light weight (few hundred solar masses) and form abundantly and early (roughly one per comoving cubic Mpc at  $z \simeq 20$ ). D.C. seeds are more massive ( $10^4 - 10^6$  solar masses), but rarer (a peak density of 0.1 per comoving cubic Mpc at  $z \simeq 12$ ). We summarize below the relevant and standard assumptions that go into our modeling of SMBH growth.

Essentially in this scheme central SMBHs hosted in galaxies accumulate mass via accretion episodes that are triggered by galaxy mergers. Accretion proceeds in one of two modes: self-regulated or un-regulated. For each SMBH in our models we know its mass at the time when the merger starts ( $M_{\text{in}}$ ), and we set the final mass through the self-regulated or un-regulated prescription. These two models differ by the amount of mass a SMBH accretes during a given accretion phase. In the context of the currently supported paradigm for structure formation, growth of structure in the Universe occurs hierarchically and via copious merging activity. Our models rely on the following assumptions:

- SMBHs in galaxies undergoing a major merger (i.e., having a mass ratio  $>1:10$ ) accrete mass and become active.
- In the self-regulated model, each SMBH accretes an amount of mass, corresponding to 90% of the mass predicted by the local  $M_{\text{BH}} - \sigma$

relation<sup>62</sup>,

$$M_{\text{fin}} = M_{\text{in}} + 0.9 \times 1.3 \times 10^8 \left( \frac{\sigma}{200 \text{ km s}^{-1}} \right)^{4.24} M_{\odot}; \quad (4)$$

the 90% normalization was chosen to take into account the contribution of mergers, without largely exceeding the mass given by the  $M_{\text{BH}} - \sigma$  relation for SMBHs at  $z = 0$ . Here  $\sigma$  is the velocity dispersion of the host after the merger. We adopt  $\sigma = V_c/\sqrt{3}$ , where  $V_c$  is the virial velocity of the host dark matter halo<sup>63,64</sup>. A SMBH is assumed to stop accreting once it reaches the value given by the  $M_{\text{BH}} - \sigma$  relation.

- In the unregulated mode ( $\times 2$ ) we simply set  $M_{\text{fin}} = 2 \times M_{\text{in}}$ , that is, we double the mass during each accretion episode.

- The rate at which mass is accreted scales with the Eddington rate ( $f_{\text{Edd}}$ ) for the SMBH, where  $f_{\text{Edd}}$  is the accretion rate in units of the Eddington rate. We adopt  $f_{\text{Edd}} = 0.3$  for D.C. models and  $f_{\text{Edd}} = 1$  for Pop III models in order to reproduce the mass density at  $z = 0$ . As Pop III seeds are lighter, they need to accrete more mass over the course of their cosmic history to become supermassive.

- The lifetime of an AGN depends on how much mass it accretes during each episode. Given the initial mass of a SMBH,  $M_{\text{in}}$ , and the amount of mass it accretes, we can calculate its final mass,  $M_{\text{fin}}$ , at the end of the active phase (Equation 4). For a given Eddington fraction,  $f_{\text{Edd}}$ , the mass of the SMBH grows with time as:

$$M_{\text{fin}} = M_{\text{in}} \exp \left( f_{\text{Edd}} \frac{1 - \epsilon}{\epsilon} \frac{t}{t_{\text{Edd}}} \right) \quad (5)$$

where  $\epsilon$  is the radiative efficiency ( $\epsilon \simeq 0.1$ ),  $t_{\text{Edd}} = M_{\text{BH}} c^2 / L_{\text{Edd}} = \frac{\sigma_T c}{4\pi G m_p} \simeq 0.45 \text{ Gyr}$  ( $c$  is the speed of light,  $\sigma_T$  is the Thomson cross section,  $m_p$  is the proton mass). Given  $M_{\text{in}}$  and  $M_{\text{fin}}$ , then a SMBH is active for a time  $t_{\text{AGN}} = \frac{t_{\text{Edd}}}{f_{\text{Edd}}} \frac{\epsilon}{1 - \epsilon} \ln(M_{\text{fin}}/M_{\text{in}})$ . Note that the unregulated prescription (a SMBH mass doubles at each accretion episode) corresponds to assuming that all SMBHs shine as AGN for the same time at a fixed accretion rate (e.g., 100 Myr for an accretion rate  $f_{\text{Edd}} = 0.3$ ).

In summary, we study and compare two self-regulated models (Pop III,  $f_{\text{Edd}} = 1$ ; D.C.,  $f_{\text{Edd}} = 0.3$ ) and two unregulated models (Pop III,  $f_{\text{Edd}} = 1, \times 2$ ; D.C.,  $f_{\text{Edd}} = 0.3, \times 2$ ). We use these models to derive the mass density in black holes in a cosmic volume, by summing over all existing black holes at a given redshift and normalizing by the comoving volume. We also calculate number counts (Figure 2 in the main article) imposing selection criteria that match the observations we have analyzed. The limiting luminosity is  $4.2 \times 10^{41} \text{ erg s}^{-1}$  for the stacked sample, i.e., if all the galaxies are emitting at this limit then we should detect them in the stack. For a single source, the more appropriate limit is this value multiplied by the number of sources in the stack, which is equivalent to a single source contributing all the signal. In that case, the luminosity limit is  $3.1 \times 10^{43} \text{ erg s}^{-1}$  and the flux limit is  $4.95 \times 10^{-17} \text{ erg cm}^{-2} \text{ s}^{-1}$ . In that case, the source will be individually detected. We therefore select all accreting black holes in the theoretical sample at  $z > 6$  that meet this flux criterion. From the Eddington ratio we calculate the bolometric luminosity and then apply a K-correction of 25 to derive the X-ray flux at the appropriate redshift.

### Comparison with AGN Luminosity Functions

We first compare the observational results presented with the expectations from integrating existing measurements or extrapolations of the observed AGN luminosity functions from earlier work. Integrating the hard X-ray LF<sup>40</sup> from  $z=7$  to 10 we obtain an integrated luminosity density of  $2.3 \times 10^{46} \text{ erg s}^{-1} \text{ deg}^{-2}$ , in good agreement with the values obtained from the stacking in the hard X-ray band, which are less affected by obscuration. In contrast, from the LF of  $z \sim 6$  quasars<sup>57</sup>, we expect a steep decline in the AGN number density.

Comparison of observations of the accreted SMBH mass density with predictions obtained from extrapolations of existing AGN luminosity functions to high redshifts and/or low luminosities provides contrasting results.

While there is in general good agreement up to  $z \sim 3$ , differences of up to  $\sim 2$  orders of magnitude are found at  $z > 6$ . This can be explained as the luminosity functions of Hopkins et al.<sup>56</sup> and Willott et al.<sup>57</sup> incorporate a density evolution of the form  $10^{-0.47z}$ , which is required to account for the observed evolution of the highest luminosity quasars at  $z \sim 5-6$  in the SDSS<sup>65</sup>. A similarly steep evolution from  $z \sim 3$  to  $z \sim 5$  has been reported, based on a compilation of *Chandra* X-ray observations<sup>55</sup>. However, it is worth pointing out that the accreted SMBH mass density inferred from this LF, presented in Figure S6 is significantly lower than observations and other LFs at all redshifts, which may be explained by the relatively high spectroscopic incompleteness ( $\sim 50\%$ ) of this sample. Incompleteness is a particularly important issue and limitation at high redshift, where sources are faint in the optical bands. In contrast, the AGN LF of Treister et al.<sup>58</sup> is in good agreement with the observations at all redshifts, and it is therefore the only one plotted in Figure 1 of the main paper. This work is based on the Ueda et al.<sup>40</sup> hard X-ray AGN LF modified to incorporate an increasing number of obscured sources with increasing redshift<sup>43</sup> and reducing the relative number of Compton-thick sources by a factor of  $\sim 4$ , consistent with the observed space density of these sources in the all-sky *INTEGRAL* and *Swift* surveys.

Explaining the accreted SMBH density at  $z > 6$  inferred from X-ray stacking observations would require that the comoving space density of low-luminosity AGN,  $L_X < 10^{44}$  erg s<sup>-1</sup>, remains nearly constant up to  $z \sim 3$ <sup>40</sup>. At the same time, the discrepancy with the observed density of high-luminosity sources in optical surveys can be resolved if there is a strong evolution in the number of high-luminosity sources. For example, a decline in the number of quasars with redshift given by  $10^{-0.47z}$  has been measured<sup>57</sup>. In this case, the contribution from high-luminosity sources to the integrated accreted black hole mass density will be very small,  $\sim 1-2\%$ . Alternatively, the observed results could be explained if the relative number of heavily-obscured quasars increases strongly with redshift, as measured up to  $z \sim 3$ <sup>66</sup>.

### Implications for re-ionization

Two sources of UV radiation are expected to contribute to re-ionization: star forming galaxies and quasars<sup>67-69</sup>. The conventional view is that galaxies dominate hydrogen re-ionization occurring at high redshift<sup>70</sup>,  $z \simeq 9$ , and quasars dominate helium re-ionization occurring at a later time,  $z \simeq 3$ <sup>69</sup>. This result is based on optically-selected quasar luminosity functions<sup>56,57</sup> that show, as discussed in the previous section, a steep drop of the quasar population at  $z > 4$ <sup>71</sup>. However, in ab initio models of black hole evolution through cosmic history<sup>72</sup> the amount of black hole growth required to explain the bright end of the luminosity function of quasars at  $z = 3 - 6$  implies a substantial contribution of quasars to hydrogen re-ionization, provided that UV and X-ray radiation can escape into the intergalactic medium. Our findings resolve this tension, as regardless of the amount of accretion occurring onto black holes, the bulk of the emission from the population is obscured, and UV photons cannot escape. In  $4\pi$  Compton thick sources only the highest energy photons can escape. We provide a simple estimate here of the contribution of Compton thick quasars to re-ionization. From our models we can extract information on  $d\rho$ , the accreted mass density on black holes as a function of cosmic time (Figure 1 in the main article shows the integral quantity). Let us assume, optimistically, that an escape fraction  $f_{esc} = 0.04$  of the bolometric luminosity (here we just assume  $f_{esc} = 1/k_{corr}$ ) goes into hard X-ray photons with mean energy  $E_\gamma = 10$  keV that can escape from the quasar host. All these photons contribute to primary and secondary ionizations. The number of ionizing photons per hydrogen atom can be evaluated from the following differential equation:

$$dx = \frac{f_{esc}}{\rho_H E_\gamma} d\rho + \frac{f_{SI}(x)}{\rho_H 14.4 \text{eV}} d\rho - x \frac{dt}{t_{rec}}, \quad (6)$$

where  $\rho_H$  is the hydrogen cosmic density<sup>70</sup>, and the recombination timescale for hydrogen is  $t_{rec} \simeq 0.3[(1+z)/4]^{-3}$  Gyr<sup>69</sup>. Here the first term of the right hand side of the equation includes primary ionizations by ionizing photons, the second term accounts for secondary ionizations from energetic ionizing photons<sup>72-74</sup>, and the third term accounts for recombinations. Here  $f_{SI}(x) \approx 0.35(1 - x^{0.4})^{1.8} - 1.77 \left(\frac{28 \text{eV}}{E_\gamma}\right)^{0.4} x^{0.2} (1 - x^{0.4})^2$ , as long as  $x < 1$ , and  $x$  is less than unity in all our models down to  $z \simeq 1$ .

The number of ionizing photons per hydrogen atom is shown in the accompanying Figure S7, where we see that models that successfully reproduce our observations **fail** to reionize hydrogen by 2-3 orders of magnitude at  $z > 6$ , notwithstanding significant black hole growth. Without taking obscuration into account, these accreting black holes would contribute substantially to re-ionization, producing one ionizing photon per atom by  $z = 6$ <sup>72</sup>.

However, we stress here that if quasars do not contribute to hydrogen re-ionization, it is not because quasar activity drops steeply at  $z > 4$  as previously suggested<sup>71</sup>, but instead due to the presence of obscuring material that absorbs UV and soft X-ray radiation. As seen in Figure S7, the models that are consistent with the observations at  $z > 6$  and include self-regulation under-produce ionizing photons at these epochs. Hence, re-ionization of the early Universe is most likely due to star forming galaxies and not growing black holes. However, this is still vigorously debated. As previously shown<sup>75</sup>, observed  $z \sim 7$  galaxies cannot provide enough hydrogen-ionizing photons unless some of the galaxy properties, such as escape fraction, metallicity, initial stellar mass function or dust extinction, evolve significantly from  $z \sim 7$  to the local Universe. Similarly, the extrapolation of the galaxy luminosity function at the faint end plays a major role in whether these sources can re-ionize the Universe<sup>76</sup>.

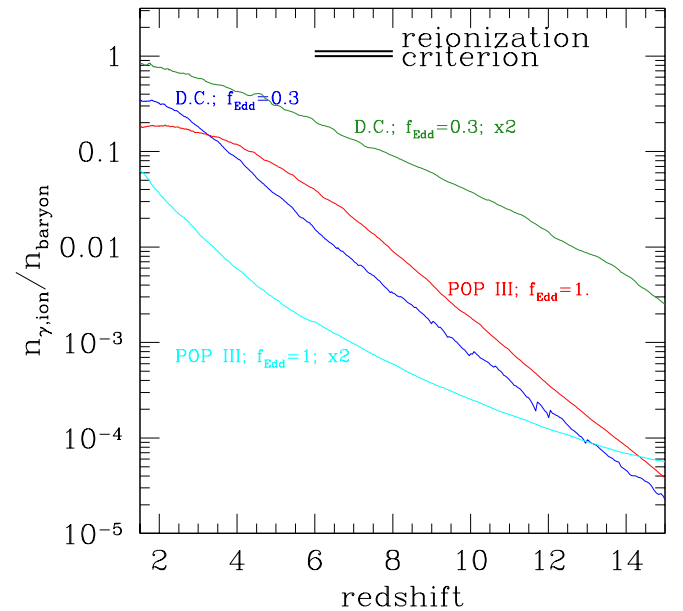


**Figure 7** | Number of ionizing photons per hydrogen atom. Models are labelled in the figure (Pop III,  $f_{Edd} = 1$ ; Pop III,  $f_{Edd} = 1, \times 2$ ; D.C.,  $f_{Edd} = 0.3$ ; D.C.,  $f_{Edd} = 0.3, \times 2$ ). A ratio of at least one ionizing photon per hydrogen atom is required to re-ionize the Universe. As can be seen in this figure, most models predict a ratio for the early growing black holes that is lower than this value by 2-3 orders of magnitude at  $z > 6$ .

## References

31. Bouwens, R. J., Illingworth, G. D., Blakeslee, J. P. & Franx, M. Galaxies at  $z \sim 6$ : The UV Luminosity Function and Luminosity Density from 506 HUDF, HUDF Parallel ACS Field, and GOODS i-Dropouts. *Astrophys. J.* **653**, 53–85 (2006).
32. Bouwens, R. J. *et al.* UV Luminosity Functions from 113  $z \sim 7$  and  $z \sim 8$  Lyman-Break Galaxies in the ultra-deep HUDF09 and wide-area ERS WFC3/IR Observations. *ArXiv e-prints*, 1006.4360 (2010).
33. Vanzella, E. *et al.* Spectroscopic Observations of Lyman Break Galaxies at Redshifts  $\sim 4, 5$ , and 6 in the GOODS-South Field. *Astrophys. J.* **695**, 1163–1182 (2009).
34. Vanzella, E. *et al.* Spectroscopic confirmation of two Lyman break galaxies at redshift beyond 7. *Astrophys. J. in press*, arXiv:1011.5500 (2010).
35. Lehnert, M. D. *et al.* Spectroscopic confirmation of a galaxy at redshift  $z = 8.6$ . *Nature* **467**, 940–942 (2010).
36. Data publicly available at <http://cxc.harvard.edu/cda/Contrib/CDFS.html>.
37. Alexander, D. M. *et al.* The Chandra Deep Field North Survey. XIII. 2 Ms Point-Source Catalogs. *Astron. J.* **126**, 539–574 (2003).
38. Nandra, K., George, I. M., Mushotzky, R. F., Turner, T. J. & Yaqoob, T. ASCA Observations of Seyfert 1 Galaxies. I. Data Analysis, Imaging, and Timing. *Astrophys. J.* **476**, 70– (1997).
39. Ueda, Y. *et al.* Suzaku Observations of Active Galactic Nuclei Detected in the Swift BAT Survey: Discovery of a “New Type” of Buried Supermassive Black Holes. *Astrophys. J.* **664**, L79–L82 (2007).
40. Ueda, Y., Akiyama, M., Ohta, K. & Miyaji, T. Cosmological Evolution of the Hard X-Ray Active Galactic Nucleus Luminosity Function and the Origin of the Hard X-Ray Background. *Astrophys. J.* **598**, 886–908 (2003).
41. La Franca, F. *et al.* The HELLAS2XMM Survey. VII. The Hard X-Ray Luminosity Function of AGNs up to  $z = 4$ : More Absorbed AGNs at Low Luminosities and High Redshifts. *Astrophys. J.* **635**, 864–879 (2005).
42. Sazonov, S., Revnivtsev, M., Krivonos, R., Churazov, E. & Sunyaev, R. Hard X-ray luminosity function and absorption distribution of nearby AGN: INTEGRAL all-sky survey. *Astron. Astrophys.* **462**, 57–66 (2007).
43. Treister, E. & Urry, C. M. The Evolution of Obscuration in Active Galactic Nuclei. *Astrophys. J.* **652**, L79–L82 (2006).
44. Ballantyne, D. R., Everett, J. E. & Murray, N. Connecting Galaxy Evolution, Star Formation, and the Cosmic X-Ray Background. *Astrophys. J.* **639**, 740–752 (2006).
45. Gilli, R. *et al.* A Compton-thick AGN at  $z \sim 5$  in the 4 Ms Chandra Deep Field South. *Astrophys. J. in press*. (2011). arXiv:1102.4714.
46. Soltan, A. Masses of quasars. *Mon. Not. R. Astron. Soc.* **200**, 115–122 (1982).
47. Yu, Q. & Tremaine, S. Observational constraints on growth of massive black holes. *Mon. Not. R. Astron. Soc.* **335**, 965–976 (2002).
48. Marconi, A. *et al.* Local supermassive black holes, relics of active galactic nuclei and the X-ray background. *Mon. Not. R. Astron. Soc.* **351**, 169–185 (2004).
49. Barger, A. J. *et al.* The Cosmic Evolution of Hard X-Ray-selected Active Galactic Nuclei. *Astron. J.* **129**, 578–609 (2005).
50. Elvis, M. *et al.* Atlas of quasar energy distributions. *Astrophys. J.* **95**, 1–68 (1994).
51. Natarajan, P. & Treister, E. Is there an upper limit to black hole masses? *Mon. Not. R. Astron. Soc.* **393**, 838–845 (2009).
52. Steffen, A. T. *et al.* The X-Ray-to-Optical Properties of Optically Selected Active Galaxies over Wide Luminosity and Redshift Ranges. *Astron. J.* **131**, 2826–2842 (2006).
53. Shankar, F., Weinberg, D. H. & Miralda-Escudé, J. Self-Consistent Models of the AGN and Black Hole Populations: Duty Cycles, Accretion Rates, and the Mean Radiative Efficiency. *Astrophys. J.* **690**, 20–41 (2009).
54. Treister, E., Urry, C. M., Schawinski, K., Cardamone, C. N. & Sanders, D. B. Heavily Obscured Active Galactic Nuclei in High-redshift Luminous Infrared Galaxies. *Astrophys. J.* **722**, L238–L243 (2010).
55. Silverman, J. D. *et al.* The Luminosity Function of X-Ray-selected Active Galactic Nuclei: Evolution of Supermassive Black Holes at High Redshift. *Astrophys. J.* **679**, 118–139 (2008).
56. Hopkins, P. F., Richards, G. T. & Hernquist, L. An Observational Determination of the Bolometric Quasar Luminosity Function. *Astrophys. J.* **654**, 731–753 (2007).
57. Willott, C. J. *et al.* The Canada-France High- $z$  Quasar Survey: Nine New Quasars and the Luminosity Function at Redshift 6. *Astron. J.* **139**, 906–918 (2010).
58. Treister, E., Urry, C. M. & Virani, S. The Space Density of Compton Thick AGN and the X-ray Background. *Astrophys. J.* **696**, 110–120 (2009).
59. Volonteri, M., Haardt, F. & Madau, P. The Assembly and Merging History of Supermassive Black Holes in Hierarchical Models of Galaxy Formation. *ApJ* **582**, 559–573 (2003).
60. Volonteri, M. & Natarajan, P. Journey to the  $M_{BH}-\sigma$  relation: the fate of low-mass black holes in the Universe. *Mon. Not. R. Astron. Soc.* **400**, 1911–1918 (2009).
61. Volonteri, M. & Begelman, M. C. Quasi-stars and the cosmic evolution of massive black holes. *Mon. Not. R. Astron. Soc.* **409**, 1398– (2010).
62. Gültekin, K. *et al.* The  $M-\sigma$  and  $M-L$  Relations in Galactic Bulges, and Determinations of Their Intrinsic Scatter. *Astrophys. J.* **698**, 198–221 (2009).
63. Ferrarese, L. Beyond the Bulge: A Fundamental Relation between Supermassive Black Holes and Dark Matter Halos. *Astrophys. J.* **578**, 90–97 (2002).
64. Kormendy, J. & Freeman, K. C. Scaling Laws for Dark Matter Halos in Late-Type and Dwarf Spheroidal Galaxies. In S. Ryder, D. Pisano, M. Walker, & K. Freeman (ed.) *Dark Matter in Galaxies*, vol. 220 of *IAU Symposium*, 377– (2004).
65. Fan, X. *et al.* High-Redshift Quasars Found in Sloan Digital Sky Survey Commissioning Data. IV. Luminosity Function from the Fall Equatorial Stripe Sample. *Astron. J.* **121**, 54–65 (2001).
66. Treister, E. *et al.* Major Galaxy Mergers and the Growth of Supermassive Black Holes in Quasars. *Science* **328**, 600– (2010).
67. Shapiro, P. R. & Giroux, M. L. Cosmological H II regions and the photoionization of the intergalactic medium. *Astrophys. J.* **321**, L107–L112 (1987).
68. Haardt, F. & Madau, P. Radiative Transfer in a Clumpy Universe. II. The Ultraviolet Extragalactic Background. *Astrophys. J.* **461**, 20– (1996).
69. Madau, P., Haardt, F. & Rees, M. J. Radiative Transfer in a Clumpy Universe. III. The Nature of Cosmological Ionizing Sources. *Astrophys. J.* **514**, 648–659 (1999).
70. Spergel, D. N. *et al.* Three-Year Wilkinson Microwave Anisotropy Probe (WMAP) Observations: Implications for Cosmology. *Astrophys. J.* **170**, 377–408 (2007).
71. Faucher-Giguère, C., Lidz, A., Hernquist, L. & Zaldarriaga, M. Evolution of the Intergalactic Opacity: Implications for the Ionizing Background, Cosmic Star Formation, and Quasar Activity. *Astrophys. J.* **688**, 85–107 (2008).
72. Volonteri, M. & Gnedin, N. Y. Relative Role of Stars and Quasars in Cosmic Reionization. *Astrophys. J.* **703**, 2113–2117 (2009).
73. Shull, J. M. & van Steenberg, M. E. X-ray secondary heating and ionization in quasar emission-line clouds. *Astrophys. J.* **298**, 268–274 (1985).
74. Madau, P., Rees, M. J., Volonteri, M., Haardt, F. & Oh, S. P. Early Reionization by Miniquasars. *Astrophys. J.* **604**, 484–494 (2004).
75. Ouchi, M. *et al.* Large Area Survey for  $z = 7$  Galaxies in SDF and GOODS-N: Implications for Galaxy Formation and Cosmic Reionization. *Astrophys. J.* **706**, 1136–1151 (2009).
76. Grazian, A. *et al.* A critical analysis of the UV Luminosity Function at redshift 7 from deep WFC3 data. *ArXiv e-prints*, 1011.6569 (2010).
77. Luo, B. *et al.* The Chandra Deep Field-South Survey: 2 Ms Source Catalogs. *Astrophys. J.* **179**, 19–36 (2008).
78. Gawiser, E. *et al.* The Multiwavelength Survey by Yale-Chile (MUSYC): Survey Design and Deep Public UBVRIZ’ Images and Catalogs of the Extended Hubble Deep Field-South. *Astrophys. J.* **162**, 1–19 (2006).



## Appendix A: Optimized X-ray stacking

We start by assuming that all sources are equally bright in the X-rays, with count rate  $R_s, R_h$  in cts/Ms in the soft and hard bands, respectively. The background levels in *Chandra* for the ACIS-I detectors as measured in the CDF-S 4 Msec data are  $B_s=0.049$  cts/Ms/pixel in the soft band and  $B_h=0.160$  cts/Ms/pixel in the hard one, in good agreement with the values of 0.066 cts/Ms/pixel (soft), and 0.167 cts/Ms/pixel (hard) measured in the CDF-S 2 Msec data<sup>77</sup>. The background level was found to vary by  $\sim 5\%$  (standard deviation) across the field. To account for this, the background value was determined for each source independently by measuring the average count rate on an annulus around the source position with inner radius  $2r$ , where  $r$  is the aperture radius in pixels and outer radius fixed to  $22''$ . A  $3\text{-}\sigma$  clipping was used for the background determination. Then, an aperture of radius  $r$  pixels has area  $\pi r^2$  and hence background counts  $B_k \pi r^2 < E(r) >_k$  where  $< E(r) >_k$  stands for the average of the exposure time  $E_{ij}$  over all pixels inside this aperture around the  $k$ th source and  $B_k$  is the background level for that source. The signal contained within this aperture can be found by interpolating the enclosed energy profiles, which give us the values of  $r$  corresponding to various fractions  $f$  of  $R$  as a function of offaxis angle  $\theta$ , e.g.  $r(\theta, f = 0.95)$ . We interpolate between these curves to determine the desired function,  $f(\theta, r)$ , producing a expected signal for the  $k$ th source of  $S_k = R f(\theta_k, r) < E(r) >_k$ . We assume that the noise receives Poisson contributions from both the background and the object counts,  $N_k = \sqrt{(R f(\theta_k, r) + B \pi r^2) < E_s(r) >_k}$ . Hence the signal-to-noise is given by

$$\left(\frac{S}{N}\right)_k = \frac{R f(\theta_k, r) \sqrt{\langle E(r) \rangle_k}}{\sqrt{R f(\theta_k, r) + B \pi r^2}} \quad (7)$$

For each source, we choose the value of  $r$  that maximizes this function. In our case, each individual source is dim enough that background fluctuations dominate the noise, and assuming that  $E_{ij}$  is slowly varying, the function to be maximized is just  $f(\theta_k, r)/r$ . The resulting values of  $r$  as a function of off-axis angle for the soft and hard bands are shown in Figure S3. A minimum radius of  $1''$  was assumed in order to avoid flux losses due to astrometric problems and pixel aliasing.

We will stack the estimated source count rates,  $R_k$ , rather than the observed source counts,  $C_k$ , since the latter depends on the PSF and exposure time at each source position but the former does not. This is superior to performing photometry on the stacked image, which requires using a constant aperture for all sources. The standard technique in the literature of performing photometry on the stacked image and dividing by the number of sources is both sub-optimal and biased; the bias could be fixed by instead dividing by the effective number of sources given the PSF and exposure information.

While a straightforward averaging (“stack”) of the source count rates is unbiased, it is still not optimal because it gives equal weight to each count rate even though some were measured with lower SNR. We can derive the weights that optimize  $S/N$  of the combined stack by noting that the combined stack will have  $S = \sum_i w_i S_i$  and  $N^2 = \sum_i w_i^2 N_i^2$  (since the weighted sum is just an unweighted sum of new objects with signal  $w_i S_i$  and noise  $w_i N_i$ <sup>78</sup>). It is easy to show that the optimal weight is then  $w_i = S_i/N_i^2$  which has the required behavior that multiplying all the weights by a constant  $k$  preserves the final  $S/N$ .

Then, we obtain that:

$$\frac{S}{N} = \frac{\sum_i w_i S_i}{\sqrt{\sum_i w_i^2 N_i^2}} = \frac{\sum_i S_i^2/N_i^2}{\sqrt{\sum_i S_i^2/N_i^2}} = \sqrt{\sum_i S_i^2/N_i^2} \quad (8)$$

Hence the optimal weights cause  $S/N$  to add in quadrature so it will never formally decrease. However, in practice there is little benefit to including objects that offer individual  $S/N$  of less than 10% of the typical objects in the field, which is why we only stacked sources closer than  $9'$  from the average *Chandra* aim point.